Adaptive fault feature extraction from wayside acoustic signals from train bearings

Zhang, Dingcheng; Entezami, Mani; Stewart, Edward; Roberts, Clive; Yu, Dejie

DOI:
10.1016/j.jsv.2018.04.004

Document Version
Peer reviewed version

Citation for published version (Harvard):
Zhang, D, Entezami, M, Stewart, E, Roberts, C & Yu, D 2018, 'Adaptive fault feature extraction from wayside acoustic signals from train bearings' Journal of Sound and Vibration, vol. 425, pp. 221-238. https://doi.org/10.1016/j.jsv.2018.04.004

Adaptive Fault Feature Extraction from Wayside Acoustic Signals from Train Bearings

Dingcheng zhang[1]*, Mani Entezami[1], Edward Stewart[1], Clive Roberts[1], Dejie YU[2]

1. School of Engineering, University of Birmingham, Birmingham, B152TT, United Kingdom
2. State Key Laboratory of Advanced Design and Manufacturing for Vehicle Body, Hunan University, Changsha, 410082, China

Abstract: Wayside acoustic detection of train bearing faults plays a significant role in maintaining safety in the railway transport system. However, the bearing fault information is normally masked by strong background noises and harmonic interferences generated by other components (e.g. axles and gears). In order to extract the bearing fault feature information effectively, a novel method called improved singular value decomposition (ISVD) with resonance-based signal sparse decomposition (RSSD), namely the ISVD-RSSD method, is proposed in this paper. A Savitzky-Golay (S-G) smoothing filter is used to filter singular vectors (SVs) in the ISVD method as an extension of the singular value decomposition (SVD) theorem. Hilbert spectrum entropy and a stepwise optimisation strategy are used to optimize the S-G filter's parameters. The RSSD method is able to nonlinearly decompose the wayside acoustic signal of a faulty train bearing into high and low resonance components, the latter of which contains bearing fault information. However, the high level of noise usually results in poor decomposition results from the RSSD method. Hence, the collected wayside acoustic signal must first be de-noised using the ISVD component of the ISVD-RSSD method. Next, the de-noised signal is decomposed by using the RSSD method. The obtained low resonance component is then demodulated with a Hilbert transform such that the bearing fault can be detected by observing Hilbert envelope spectra. The effectiveness of the ISVD-RSSD method is verified through both laboratory field-based experiments as described in the paper. The results indicate that the proposed method is superior to conventional spectrum analysis and ensemble empirical mode decomposition methods.

Keywords: wayside acoustic detection, train bearing, improved singular value decomposition, Savitzky-Golay smoothing filter, resonance-based signal sparse decomposition

*Corresponding author. Tel.: +44 07422941910;
E–mail address: railcm@contacts.bham.ac.uk (Dingcheng Zhang)

1 Introduction

In recent years, growth in passenger rail travel has dramatically increased. This demand has been driven by a number of factors including economic mobility, improved punctuality, and increased reliability. In order to sustain this growth, safety and reliability of railway transportation systems have become points of focus for the industry. Train bearings, are key components of the vehicle that support the whole weight of the train and operate at high speeds. Faults easily occur in train bearings and result in economic loss or even casualties. Hence, fault detection in these key components plays a significant role in maintaining and continuing to increase rail's role in transportation networks.

Recently, many technologies have been suggested as suitable candidates for monitoring train axle-bearings without needing to disassemble them for inspection. Some technologies, such as oil monitoring [1] and vibration-based detection [2,3], are vehicle-mounted. These provide high quality information but require sensors and equipment to be fitted to every bearing on every vehicle. Acoustic emission [4] and hot axle box [5] detection systems can be fitted to one location in the network, but the former requires phyical access to the track, while the latter is only suitable for detecting late stage faults [6]. Wayside acoustic detection is another technology that is becoming increasingly popular because one monitoring station will observe multiple vehicles, no physical track access is required in order to install the equipment, and detection is at an earlier stage than its thermal counterpart.

Acoustic waves are vibrational energy signals that are transmitted from the bearings via an elastic medium, i.e. through the air. If there is a fault in the axle-bearing, repeated impulse signals will occur in the vibration signal observed. Thus, train bearing faults can be detected by extracting these impulse signals. However, in this application, fault feature signals are often masked by high levels of background noise (e.g. vehicle noise, environmental noise, or aerodynamic noise, etc. [7]). Furthermore, they are also susceptible to harmonic interference.

To overcome this problem, researchers have proposed many methods. Wang et al. [8] use a variable FIR filter to obtain the fault feature signal after estimating the instantaneous frequencies. Combining the stochastic resonance method with multiscale noise tuning, He et al. [9] proposed the adaptive stochastic resonance method to enhance weak defect information. Zhang et al. [10] proposed a time-

frequency filter with thresholds to separate the wayside acoustic signal and then applied an inverse STFT to obtain a de-noised signal. These methods use a known centre frequency band to extract the fault feature signal. However, centre frequencies for fault features in wayside acoustic signals are particularly difficult to identify due to high levels of background noise and harmonic components. Additionally, the methods described above may fail to detect train bearing faults when the fault feature signals have centre frequency bands that align with strong noise components.

Using different oscillatory behaviours at different frequencies within the signal, the RSSD method can decompose the wayside acoustic signal into high resonance and low resonance components [11]. Fault feature signals generated by the bearings have low levels of oscillatory behaviour and thus the bearing fault information can be found in the low resonance component [12]. The method has been successfully demonstrated in fault diagnosis systems based on vibration analysis [13,14], however, the high levels of background noise in wayside acoustic signals normally result in poor decomposition results [15].

The singular value decomposition **(**SVD) method is the one of most commonly used denoising techniques. However, the parameter selection of the method is an intractable problem. Additionally, the traditional SVD method has limited effectiveness when the target signal has a high level of noise. To overcome these issues, the Savitzky-Golay smoothing filter used in [16] is applied to the SVs obtained by decomposing the signal using the SVD theorem. The quality of the result is, however, directly affected by the parameters of the S-G filter [17]. Hence, in this paper, envelope spectrum entropy [18,19] is introduced to construct the objective function, and the stepwise optimisation strategy (SOS) [20,21,22]is used to adaptively select the parameters of the S-G filter.

In this paper, the parameters of the SVD method are optimised so that the correct SVs can be obtained. Envelope Spectrum Entropy and a stepwise optimisation strategy are then used to adaptively select the parameters of the S-G filter. The de-noised signal is then obtained using the filtered SVs. The de-noised signal is decomposed into high and low resonance components using the RSSD method, the parameters of which are optimised using a genetic algorithm. Finally, the low resonance component is subjected to Hilbert envelope demodulation and train bearing faults can be detected by observing the Hilbert envelope spectrum. Analysis of the results of experiments presented in this paper indicates that the ISVD-RSSD method

can be used to effectively extract fault feature signals and to enhance weaker fault signals.

This paper is organised as follows: In section 2, the ISVD method is introduced. In section 3, the RSSD method is introduced. Wayside acoustic detection based on the ISVD-RSSD method is presented in section 4. In section 5, section 6 and section 7, the simulation, laboratory and field experiments' results using the proposed method are demonstrated. The conclusions of this paper are presented in the final section.

2 Improved Singular Value Decomposition for Wayside Acoustic Signal

2.1 Improved Singular Value Decomposition

A wayside acoustic signal $\mathbf{x} = (x_1, x_2, \cdots, x_N)$ can be represented as the sum of a fault feature signal $\mathbf{y} = (y_1, y_2, \cdots, y_N)$ and a noise signal $\mathrm{n} = (n_1, n_2, \cdots, n_N)$, which includes all non-fault related components (i.e. includes the sound of normal bearing operation). The Hankel matrix $\mathbf{X}$ can be constructed as shown in Eq. (1) [23].

$$\mathbf{X} = \begin{bmatrix} x_1 & x_2 & \cdots & x_m \\ x_2 & x_3 & \cdots & x_{m+1} \\ \vdots & \vdots & \ddots & \vdots \\ x_{N-m+1} & x_{N-m+2} & \cdots & x_N \end{bmatrix} \tag{1}$$

According to the SVD theorem, $\mathbf{X}$ can be factorized as

$$\mathbf{X} = \mathbf{U}\mathbf{S}\mathbf{V}^T \tag{2}$$

where $\mathbf{U} \in \mathbf{R}^{(N-m+1)\times(N-m+1)}$, $\mathbf{V} \in \mathbf{R}^{m\times m}$, and hence $\mathbf{U}^{\mathrm{T}}\mathbf{U} = \mathbf{I}_{N-m+1} = \mathbf{U}\mathbf{U}^{\mathrm{T}}$, $\mathbf{V}^{\mathrm{T}}\mathbf{V} = \mathbf{I}_m = \mathbf{V}\mathbf{V}^{\mathrm{T}}$, $\mathbf{U} = (\mathbf{u}_1, \mathbf{u}_2 \cdots, \mathbf{u}_{N-m+1})$, $\mathbf{V} = (\mathbf{v}_1, \mathbf{v}_2, \cdots, \mathbf{v}_m)$ and $\mathbf{S} = \mathrm{diag}(\sigma_1, \sigma_2, \cdots, \sigma_m)$. $\sigma_1, \sigma_2, \cdots, \sigma_m$ are known as the singular values and ordered $\sigma_1 \geq \sigma_2 \geq \cdots \geq 0$. The columns of $\mathbf{U}$ and $\mathbf{V}$, $\mathbf{u}_i$ and $\mathbf{v}_i$, are known as the left and right singular vectors (SVs) of $\mathbf{X}$. SVs can be regarded as time series. To improve the SVD method, the SVs are filtered using a Savitzky-Golay (S-G) smoothing filter as part of the ISVD method.

Hankel matrixes $\mathbf{Y}$ and $\mathbf{N}$, corresponding to the signal and noise components ($\mathbf{y}$ and $\mathbf{n}$), can also be constructed. The matrix $\mathbf{N}$ is full column rank, i.e. rank($\mathbf{N}$) = m. Thus, the rank of $\mathbf{X}$ is also equal to m, however, the rank of $\mathbf{Y}$ normally satisfies rank($\mathbf{Y}$) = k <m. Therefore, $\mathbf{X}$ and $\mathbf{Y}$ can be factorized as shown in Eq. (3) and Eq. (4):

$$\mathbf{X} = (\mathbf{U}_1\ \mathbf{U}_2)\begin{pmatrix}\mathbf{S}_1 & 0\\ 0 & \mathbf{S}_2\end{pmatrix}\begin{pmatrix}\mathbf{V}_1^T\\ \mathbf{V}_2^T\end{pmatrix} \tag{3}$$

$$\mathbf{Y} = (\bar{\mathbf{U}}_1\ \bar{\mathbf{U}}_2)\begin{pmatrix}\bar{\mathbf{S}}_1 & 0\\ 0 & 0\end{pmatrix}\begin{pmatrix}\bar{\mathbf{V}}_1^T\\ \bar{\mathbf{V}}_2^T\end{pmatrix} \tag{4}$$

where $\mathbf{U}_1, \bar{\mathbf{U}}_1 \in \mathbf{R}^{(N-m+1)\times k}$, $\mathbf{S}_1, \bar{\mathbf{S}}_1 \in \mathbf{R}^{k\times k}$, $\mathbf{V}_1, \bar{\mathbf{V}}_1 \in \mathbf{R}^{m\times k}$, $\mathbf{U}_2, \bar{\mathbf{U}}_2 \in \mathbf{R}^{(N-m+1)\times(m-k)}$, $\mathbf{S}_2 \in \mathbf{R}^{(m-k)(m-k)}$, $\mathbf{V}_2, \bar{\mathbf{V}}_2 \in \mathbf{R}^{m\times(m-k)}$. $\mathbf{S}_1$ and $\mathbf{S}_2$ can be calculated from [24]

$$\begin{cases}\mathbf{S}_1 = (\bar{\mathbf{S}}_1^2 + \sigma_w^2 \mathbf{I}_k)^{1/2}\\ \mathbf{S}_2 = \sigma_w \mathbf{I}_{m-k}\end{cases} \tag{5}$$

where σ_w satisfies $\mathbf{N}\mathbf{N}^{\mathrm{T}} = \sigma_w \mathbf{I}_{\mathrm{m}}$. Eq. (5) shows that the first k singular values in $\mathbf{S}$ are influenced by the fault feature signal and the noise signal simultaneously, while the other singular values in $\mathbf{S}$ are only influenced by the noise signal. Thus, the denoised signal $\bar{\mathbf{x}}$ can be obtained using the inverse SVD method as Eq. (6).

$$\bar{\mathbf{x}} = \sum_{i=1}^{k} \sigma_i u_i v_i^T \tag{6}$$

2.2 Parameter Selection

Four main parameters directly affect the result of the ISVD method: the embedding dimension *m*, the rank of the best approximation matrix $\bar{\mathbf{S}}_1$, the degree of the Savitzky-Golay filter d , and the window size of the S-G filter n_W . Adaptive selection methods for these parameters are proposed in this paper. A fault feature signal, $x(t)$, is used to demonstrate the selection method [25]. The signal assumes a constant shaft speed, as the time that the bearing passes the microphone is too short for any significant change in speed.

$$x(t) = \sum_{m=0}^{M-1} A_m \exp[-\beta(t - m\mathrm{T})] \times \cos[2\pi f_{re} \times (t - m\mathrm{T})] u(t - m\mathrm{T}) \tag{7}$$

where M is the number of impulses in the signal, A_m is the amplitude of the m-th impulse, and β is the impulse damping ratio. To simulate the impulse interval, the fault feature frequency f_o satisfies $f_o = 1/T$. f_{re} is the resonance frequency of the bearing, and $u(\mathrm{t})$ is the unit step function. The values of each parameter are shown in Table 1, and the fault feature signal is shown in Figure 1. The sampling frequency and

time of the simulation signal are 4096 Hz and 1 s, respectively. A simulated acoustic bearing signal, including the fault feature signal and 0 dB signal-to-noise ratio ($SNR_{Original}$), can be obtained by adding a random Gaussian noise signal to the simulated fault feature signal.

Please insert the Table 1 into here

Please insert the Figure 1 into here

2.2.1 Embedding Dimension

A novel false neighbour method [26] is introduced to determine the value of the embedding dimension *m* in the ISVD method. According to the false neighbour method, any two points which stay close in the *d*-dimension reconstructed space will be close in the (*d*+1)-dimensional reconstruction space. Such a pair of points are called true neighbours, otherwise, they are regards as false neighbours. Optimal embedding means that there are no false neighbours. Eq. (8) is constructed to find a false neighbour. If $a(i,m)$ is larger than a given threshold value, false neighbours can be identified.

$$a(i,m)=\frac{\left\|X_i(m+1)-X_{n(i,m)}(m+1)\right\|}{\left\|X_i(m)-X_{n(i,m)}(m)\right\|} \tag{8}$$

where $\|\bullet\|$ is the Euclidean norm. $X_i(m+1)$ is the i -th reconstructed vector with embedding dimension $m+1$, i.e. $X_i(m+1)=(x_i,x_{i+1},\cdots,x_{i+m})$. $X_{n(i,m)}(m)$ is the nearest neighbour of $X_i(m)$ in the m-dimensional reconstructed space $(1\le n(i,m)\le N-m)$.

To determine the threshold value, a criteria parameter $E(m)$ which is the mean value of $a(i,m)$ is defined as Eq. (9). Thus, $E(m)$ is dependent only on the dimension m . The variation from m to $m+1$ is defined as Eq. (10)

$$E(m)=\frac{1}{N-m}\sum_{i=1}^{N-m}a(i,d) \tag{9}$$

$$E1(m) = E(m+1)/E(m) \tag{10}$$

The optimal value for m, m_o, can be found when $E1(m)$ is slowly changing, defined as $|E1(m_o+1) - E1(m_o)| < 0.01$ in this paper and shown in Figure 2 (a).

2.2.2 Rank of the best approximation $\bar{\mathbf{S}}_1$

The first singular value σ_1, which corresponds to the main fault information, is bigger than other singular values as shown in Figure 2 (b). Therefore, the first singular value in $\mathbf{S}$ is retained and the other singular values are set to 0 in the ISVD method. The de-noised signal $\bar{\mathbf{x}}$ can be obtained

$$\bar{\mathbf{x}} = \sigma_1 \mathbf{u}_1 \mathbf{v}_1^T \tag{11}$$

Thus, only $\mathbf{U}(:,1)$ and $\mathbf{V}(:,1)$ in Eq. (2) need to be filtered by the S-G filter, which is computationally efficient in comparison with the method presented in reference [15].

Please insert the Figure 2 into here

2.2.3 Degree and Window Size of the Savitzky-Golay filter

In this paper, a stepwise optimisation strategy is applied to the adaptive selection of the degree (d) and window size (n_W) of the S-G filter. This strategy is widely used to solve the multi-variable optimisation problem by turning a multi-variable problem into several sub-problems by dividing variables into groups [20,21,22]. In this paper, the window size is first optimised with the degree fixed as 3. The degree is then optimised with the window size fixed as the value obtained in the first step (The maximum value of n_W is 25).

The objective function F is

$$F = ESE(\bar{\mathbf{x}}) \tag{12}$$

where $ESE(\bar{\mathbf{x}})$ is the Envelope Spectrum Entropy of the de-noised signal $\bar{\mathbf{x}}$. The ESE, as shown in Eq. (13-16), normally decreases as fault information increases [18,19]. Hence, the optimal values for the degree and window size of the S-G filter can be obtained when minimising Eq. (16) by using a stepwise optimisation strategy.

$$Z(t) = \sqrt{\bar{x}^2(t) + \mathrm{H}^2[\bar{x}(t)]} \tag{13}$$

$$Q = \left|\mathrm{FFT}(Z(t)\right| \tag{14}$$

$$B = Q / sum(Q) \tag{15}$$

$$ESE(\bar{\mathbf{x}}) = -\sum_{K=1}^{N/2} B(k) \times \log_2(B(k)) \tag{16}$$

where $\mathrm{H}[\bullet]$ and $\mathrm{FFT}(\bullet)$ represent the Hilbert transform and Fourier transform, respectively. B is the normalisation of the envelope spectrum Q. The optimisation process is shown in Eq. (17).

$$\begin{aligned} &\min \ F(d, n_W) \\ &\mathrm{s.t.}\, n_W \in \{2k+1 : k \in Z\} \\ &\quad n_W > d+1 \end{aligned} \tag{17}$$

A comparison of the ISVD and conventional methods is provided in Table 2, where de-noising results for 4 signals with different SNR (signal to noise ratios) are presented. Signal4 from the table is the simulated acoustic bearing signal generated in Section 1.2 above, and Signals1-3 are variants of this signal with different signal to noise ratios. $\mathrm{SNR_{EEMD}}$, $\mathrm{SNR_{LPSR}}$, $\mathrm{SNR_{SVD}}$ and $\mathrm{SNR_{ISVD}}$ represent the SNR for the obtained de-noised signals after using the ensemble empirical mode decomposition (EEMD) method [27], the large parameter stochastic resonance (LPSR) method [28], conventional SVD method [29] and the ISVD method respectively. The results demonstrate a significant improvement in SNR when using the ISVD method over the conventional approaches.

Please insert the Table 2 into here

3 Resonance-Based Sparse Signal Decomposition

In Section 2, the ISVD method is introduced for the purposes of de-noising acoustic signals. However, fault features in the de-noised signal can still be masked by harmonic interference. Thus, in this paper, the resonance-based sparse signal decomposition (RSSD) method is introduced to exclude these harmonic components. According to different oscillatory behaviour, the RSSD method can be used to decompose the analysis signal into the high and the low resonance components. The high resonance component is a signal consisting of multiple simultaneous sustained oscillations and the low resonance component is a signal consisting of non-oscillatory transient of unspecified shape and duration [11]. The harmonic components in the

denoised signal exhibit sustained oscillatory behavior and hence can be separated into the high resonance component. In contrast, the periodic impulse signal generated by bearing faults can be found in low resonance component [12,13].

For the RSSD method, two tunable-Q wavelet transforms (TQWT) [11] are used to represent two different signal components with different oscillatory behaviors, as described by quality factor Q. Morphological component analysis (MCA) [30] is then used to minimize the objective function for signal decomposition using the split augmented Lagrangian shrinkage algorithm (SALSA) [31].

The TQWT is actually a two-channel bandpass filter bank with real-valued scaling factors. Three levels of the TQWT analysis filter and synthesis filter are shown in Figure 3 (a) and (b), respectively. The low-pass filter $H_0(\omega)$ and the high-pass filter $H_1(\omega)$are constructed as follows Eq. (18) and (19).

$$H_0(\omega)=\begin{cases}1 & |\omega|\le(1-\beta)\pi \\ \theta(\dfrac{\omega+(\beta-1)\pi}{\alpha+\beta-1}) & (1-\beta)\pi\le\omega<\alpha\pi \\ 0 & \alpha\pi\le|\omega|<\pi\end{cases} \tag{18}$$

$$H_1(\omega)=\begin{cases}0 & |\omega|\le(1-\beta)\pi \\ \theta(\dfrac{\alpha\pi-\omega}{\alpha+\beta-1}) & (1-\beta)\pi\le\omega<\alpha\pi \\ 1 & \alpha\pi\le|\omega|<\pi\end{cases} \tag{19}$$

where $\theta(\cdot)$ is a function, for $|\upsilon|\le\pi$, $\theta(\upsilon)=0.5(1+\cos\upsilon)\sqrt{2-\cos\upsilon}$. Eq. (18) and Eq. (19) show that the low-pass and high-pass filters are determined by the low pass, α, and high pass, β, scaling parameters. The pair of scaling parameters (α, β) should satisfy Eq. (20). r is the redundancy of the TQWT, i.e. the oversampling rate of subbands of the two-channel filter bank.

$$\begin{aligned}&\beta=\frac{2}{Q+1},\ \alpha=1-\frac{\beta}{r} \\ &s.t.\ \ 0<\alpha<1,\ \ 0<\beta\le1,\ \ \ \alpha+\beta>1\end{aligned} \tag{20}$$

Please insert the Figure 3 into here

Hence, the result of the TQWT depends on the selection of quality factor, Q, and the redundancy, r. Also, in order to include all information from the analysis signal, a maximum decomposition level for the TQWT of $L_{\max}$ is used in this paper.

$$L_{\max} = \left\lfloor \frac{\log\left(\frac{N}{4(Q+1)}\right)}{\log\left(\frac{Q+1}{Q+1-2/r}\right)} \right\rfloor \tag{21}$$

Suppose that the collected wayside acoustic signal, x, can be represented as

$$\mathbf{x} = \mathbf{x}_1 + \mathbf{x}_2 + \mathbf{n} \tag{22}$$

where $\mathbf{x}_1$ is the harmonic interference component with high oscillatory behavior; $\mathbf{x}_2$ is the bearing fault feature component which has low oscillatory behavior; and $\mathbf{n}$ is the noise.

In order to estimate $\mathbf{x}_1$ and $\mathbf{x}_2$ individually, the sparse representation bases $\mathbf{\Phi}_1$ and $\mathbf{\Phi}_2$ based on two TQWTs with different oscillatory behaviors are constructed. Two coefficients $\mathbf{w}_1$ and $\mathbf{w}_2$ are then chosen such that the error of the reconstructed signal, $\mathbf{x}-\mathbf{\Phi}_1\mathbf{w}_1-\mathbf{\Phi}_2\mathbf{w}_2$, satisfies a threshold, ε, which is related to the noise energy in the signal, $\mathbf{x}$. Thus, $\mathbf{w}_1$ and $\mathbf{w}_2$ can be estimated as follows

$$\arg\min_{\mathbf{w}_1,\mathbf{w}_2} \|\mathbf{w}_1\|_1 + \|\mathbf{w}_2\|_1 \qquad s.t. \|\mathbf{x}-\mathbf{\Phi}_1\mathbf{w}_1-\mathbf{\Phi}_2\mathbf{w}_2\|_2 \le \varepsilon \tag{23}$$

Eq. (23) can be replaced by the unconstrained minimization below

$$\arg\min_{\mathbf{w}_1,\mathbf{w}_2} \|\mathbf{x}-\mathbf{\Phi}_1\mathbf{w}_1-\mathbf{\Phi}_2\mathbf{w}_2\|_2^2 + \lambda_1\|\mathbf{w}_1\|_1 + \lambda_2\|\mathbf{w}_2\|_1 \tag{24}$$

where the Lagrange multipliers λ_1 and λ_2 are selected according to the power of the noise, which is calculated by Eq. (25) [32]

$$\begin{cases} \lambda_1 = \theta\|\psi_1\|_2 \\ \lambda_2 = (1-\theta)\|\psi_2\|_2 \end{cases} \tag{25}$$

where θ has an effect on the energy distribution between the high and low resonance components. To avoid put too much energy into one of the two components, and too little into the other, in this paper θ is set to 0.5. ψ_1 and ψ_2 represent the wavelets corresponding to coefficients $\mathbf{w}_1$ and $\mathbf{w}_2$, respectively.

In the RSSD method, the SALSA method is used to solve the minimisation problem of the objective function in Eq. (24) using the following update equations

$$\mathbf{u}^{(k+1)} = soft(\mathbf{w}^{(k)} + \mathbf{d}^{(k)}, \lambda / \mu) \tag{26}$$

$$\mathbf{v}^{(k+1)} = \mathbf{u}^{(k+1)} - \mathbf{d}^{(k)} \tag{27}$$

$$\mathbf{d}^{(k+1)} = \frac{1}{\mu + 2} \mathbf{\Phi}(x - \mathbf{\Phi}^{*} \mathbf{v}^{(k+1)}) \tag{28}$$

$$\mathbf{w}^{(k+1)} = \mathbf{d}^{(k+1)} + \mathbf{v}^{(k+1)} \tag{29}$$

where $soft(\mathbf{y}, T)$ is the soft-threshold rule for the threshold T, k is the iteration number, μ is a penalty parameter, $\mathbf{\Phi} = [\mathbf{\Phi}_1, \mathbf{\Phi}_2]^T$, $\mathbf{\Phi}\mathbf{\Phi}^{*} = \mathbf{I}$, and $\mathbf{w} = [\mathbf{w}_1, \mathbf{w}_2]^T$.

After $\mathbf{w}_1$ and $\mathbf{w}_2$ are obtained, the estimated high and low resonance components are as follows

$$\hat{\mathbf{x}}_1 = \mathbf{\Phi}_1 \mathbf{w}_1^{*}, \quad \hat{\mathbf{x}}_2 = \mathbf{\Phi}_2 \mathbf{w}_2^{*} \tag{30}$$

For RSSD, 4 main parameters need to be determined, namely, the quality factor Q_1, the redundancy r_1 corresponding to the high resonance component, the quality factor Q_2, and the redundancy r_2 corresponding to the low resonance component. In this paper, a genetic algorithm (GA) is applied to the parameter optimisation for the RSSD method. The kurtosis of the low resonance component $\hat{\mathbf{x}}_2$ is taken as the evaluation index F, as shown in Eq. (31) [12]. Therefore, the adaptive selection process for the decomposition parameters of RSSD can be turned into a maximisation process for the evaluation index.

$$F = Kur(\hat{\mathbf{x}}_2) \tag{31}$$

4 Adaptive fault feature extraction of wayside acoustic signals from train bearings

In this paper, a novel method combining the Improved Signal Value Decomposition (ISVD) and Resonance-based Signal Sparse Decomposition (RSSD) methods is proposed to adaptively extract fault features for train bearings from wayside acoustic signals. In the ISVD-RSSD method, the collected wayside acoustic signals are firstly de-noised using the ISVD method before and then the de-noised signals are decomposed into high and low resonance components using the RSSD method; the low resonance component usually includes bearing fault information. Finally, the Hilbert envelope demodulation is applied to the low resonance component.

By observing the Hilbert envelope spectrum of the low resonance component, train bearing faults can be detected. A flow chart showing the proposed method is shown in Figure 4.

Please insert the Figure 4 into here

5 Simulation Experiment

To demonstrate the effectiveness of the proposed method, a synthesized signal is constructed to simulate the bearing fault. This includes a fault feature signal x_1, two harmonic signals x_2, x_3 and random noise x_4. The fault feature signal x_1 is constructed using Eq. 7 and its fault feature frequency f_0 is set as 33 Hz. The two harmonic signals, x_2 and x_3, are shown in Eq. (32) where f_1, f_2 and f_3 are set to 50 Hz, 600 Hz and 42 Hz. These values are selected based on laboratory experiments. In addition, a random Gaussian noise with SNR of -5 dB is added. The time domain waveform and the Hilbert envelope spectrum of the synthesized signal are shown in Figure 5 (a) and (b). Figure 5 shows that the bearing fault information is masked by strong harmonic interference and noise, especially the obvious peaks at f_1, f_2-f_3, $f_2-f_3-f_1$ and $f_2-f_3+f_1$ in Figure 5 (b).

$$\begin{cases} x_2 = (1+\cos(2\pi f_1 t))\cos(2\pi f_2 t)) \\ x_3 = \cos(2\pi f_3 t) \end{cases} \quad (32)$$

Please insert the Figure 5 into here

The synthesized signal is subjected to the ISVD method and the result is shown in Figure 6. Figure 6 (a) and (b) are the time domain waveform and the Hilbert envelope spectrum of the denoised signal. Comparing Figure 5 (a) and Figure 6 (a), it can be found that the noise component in the denoised signal is clearly reduced after using the ISVD method. However, the bearing fault information is still masked by the strong harmonic component, i.e. there are no obvious peaks at f_0 or its harmonics.

Please insert the Figure 6 into here

The RSSD method is applied to decompose the denoised signal as shown in Figure 6 (a) and the result is demonstrated in Figure 7. The time domain waveform and the Hilbert envelope spectrum of the high resonance component are shown as Figure 7 (a) and (b). Figure 7 (c) and (d) are the time domain waveform and the Hilbert envelope spectrum of the low resonance component. Figure 7 (d) shows that there are obvious peaks at f_o and its harmonics which indicates the existence of a bearing fault. Hence, the harmonic components and the bearing fault feature component have been separated into the high and the low resonance components respectively using the RSSD method. The effectiveness of the ISVD-RSSD method is therefore demonstrated.

Please insert the Figure 7 into here

The synthesized signal shown in Figure 5 (a) has also been analysed using ensemble empirical mode decomposition (EEMD) [27]. The first intrinsic mode function (IMF), which has the maximum kurtosis value, is selected and its time domain waveform and Hilbert envelope spectrum are shown Figure 8 (a) and (b), respectively. Figure 8 (b) shows that there is a peak at f_o, which indicates the existence of a bearing fault. However, an additional substantial peak exists at f_1 and there is no obvious peak at the harmonic frequency associated with f_o. Comparing with Figure 7 (d), it can be concluded that the method proposed in the paper is superior to the EEMD method.

Please insert the Figure 8 into here

To test the sensitivity of the proposed method, simulation signals with different noise levels are constructed. The Hilbert envelope spectra of the low resonance components are generated with different SNR values (from -7 dB to -12 dB), as shown in Figure 9. The figure shows that obvious peaks exist at f_o and its harmonic components, which are marked by red circles. This demonstrates good anti-noise capability of the proposed method.

Please insert the Figure 9 into here

6 Laboratory Experiment

Laboratory experiments have been undertaken in order to demonstrate the capability of the proposed method. In the experiments, acoustic signals are collected from bearings mounted on a test rig, as shown in Figure 10(a). The test bearing used is shown in Figure 10(b); its parameters are given in Table 3. It can be seen from Figure 10(b) that a minor fault exists in the outer race covering approximately 1.7% of the circumference. The signal from the first of the two microphones shown in the figure is used in the experiment.

Please insert the Figure 10 into here

Please insert the Table 3 into here

The sampling frequency used, f_s, is 12500 Hz. 4096 samples are recorded per measurement. The rotational frequency, f_r, is 8.3 Hz. Therefore, the frequency with which each roller passes a point on the outer race f_{RPFO} is 76.6 Hz, as indicated by Eq. (33)

$$f_{RPFO} = \frac{n}{2}(1 - \frac{RD}{PD}\cos\beta) f_r \tag{33}$$

For comparison, signals are also collected from a healthy bearing. The time domain waveforms of the collected signals and correspondingly FFT spectra for both the healthy and the faulty bearings are shown in Figure 11(a) and (b), respectively. Figure 11 shows that there are both noise and harmonic interferences in the recorded signals. Especially, the peaks at 79.35 Hz and 64.09 Hz in FFT spectra in Figure 11(a) and (b) are generated by the drive system (a DC motor, a shaft, and a connecting belt). The harmonic interference generated by the drive system are collected by the microphone. The Hilbert envelope spectra of the test signals are shown in Figure 12. The peaks at f_{RPFO} and its harmonics in the figure are masked by a combination of noise and harmonic interference. Further peaks which also exist around 720 Hz to 920 Hz are caused by the coupling of harmonic interference components in envelope

demodulation analysis. Thus, conventional spectrum analysis techniques are not appropriate for the extraction of the fault features.

Please insert the Figure 11 into here

Please insert the Figure 12 into here

The signals shown in Figure 11 (a) and (b) are subjected to the ISVD method such that the corresponding de-noised signals are shown in Figure 13 (a) and (b). Figure 14 shows the Hilbert envelope spectra of the de-noised signals. While the figures indicate good de-noising results for the ISVD method, the fault feature signals are still masked by strong harmonic components. In Figure 14, peaks at 79.35 Hz and 64.09 Hz indicate the main harmonic components for the healthy bearing and the faulty bearing, respectively. However, there is no obvious peak at f_{RPFO} or its harmonics in the Hilbert envelope spectrum of the de-noised signal for the faulty bearing.

Please insert the Figure 13 into here

Please insert the Figure 14 into here

The de-noised signals, as shown in Figure 13 (a) and (b), are decomposed using RSSD with optimised parameters; the results of which are shown in Figure 15 and Figure 16. Figure 15 (a) and (b) are the time domain waveforms and FFT spectra of the high and low resonance components for the healthy bearing, respectively. Figure 16 (a) and (b) are the time domain waveforms and FFT spectra of the high and low resonance components for the faulty bearing, respectively. It can be seen from Figure 15 (a) and Figure 16 (a) that the harmonic interference elements (with 79.35 Hz and with 64.09 Hz, respectively) are decomposed into the high resonance component. Other components with low oscillatory behaviour, such as bearing fault information, are included in the low resonance component shown in Figure 15 (b) and Figure 16 (b).

Please insert the Figure 15 into here

Please insert the Figure 16 into here

The Hilbert envelope spectra of the high and low resonance components are shown in Figure 17 and Figure 18 respectively. Figure 17 shows that the main harmonic components in the test signals, as identified in Figure 14, are decomposed into the high resonance component. Furthermore, the Hilbert envelope spectrum of the low resonance component for the faulty bearing demonstrates peaks at f_{RPFO}, $2f_{RPFO}$ and $3f_{RPFO}$, as shown in Figure 18. These indicate the presence of the outer race fault. The clear presence of the 2^{nd} and 3^{rd} harmonics of f_{RPFO} alongside the fundamental peak in the signal allows greater confidence in the association of the signals with the specific bearing geometry and thus fault detection. This increase in confidence is a key benefit derived from the use of the ISVD-RSSD method. The ISVD-RSSD parameters used in the laboratory experiment are shown in Table 4.

Please insert the Figure 17 into here

Please insert the Figure 18 into here

Please insert the Table 4 into here

In order to evaluate the significance of the ISVD component of the ISVD-RSSD algorithm, the test signal as shown in Figure 11(b) (the raw data recorded from the faulty bearing) can be directly decomposed using the RSSD method. The Hilbert envelope spectrum of the obtained low resonance component is shown in Figure 19. The figure shows that the strong noise components and residual harmonics are still present. The signal also demonstrates no obvious peaks at f_{RPFO} or its harmonics which would likely result in missed diagnosis. Hence, it can be shown that de-noising the signals, using a technique such as ISVD, prior to the application of the RSSD method is essential.

Please insert the Figure 19 into here

The raw signal from the faulty bearing, as shown in Figure 11 (b), can also be analysed using ensemble empirical mode decomposition (EEMD) [27]. The second intrinsic mode function (IMF), which has the maximum kurtosis value, is selected and shown in Figure 20. The figure demonstrates no obvious peaks at f_{RPFO} or its harmonics, which could also result in missed diagnosis. Hence the ISVD-RSSD method is considered more suitable than a basic EEMD.

Please insert the Figure 20 into here

7 Field Experiment

In order to test the performance of the ISVD-RSSD method in a real railway environment, acoustic signals were collected from the wayside as a test train was passing along a section of continuously welded (jointless) track. The test train consisted of a single car of a DMU hauling two test wagons, as shown in Figure 21(a). The speed of the test train through the monitored section was 13.1 m/s, i.e. approximately 278 RPM for a wheel size of 0.9 m. For safety reasons, it was not possible to operate a train with known faulty bearings, so instead a loudspeaker was fitted to the third axle of the train [33]. An acoustic signal recorded in the laboratory from a train bearing (TAROL 130/230-U-TVP) with a minor fault was played over the loudspeaker in order to simulate a vehicle with a bearing fault. In order to align with the speed of the train, the rotational speed used during the recording was approximately 270 RPM. The parameters of the test bearing are shown in Table 5. The roller fault frequency f_{RFF} is approximately 35 Hz as calculated using Eq. (34).

Please insert the Figure 21 into here

Please insert the Table 5 into here

$$f_{RFF} = \frac{PD}{RD}\left(1-\left(\frac{RD}{PD}\cos\beta\right)^2\right) f_r \tag{34}$$

A wayside acoustic monitoring system as illustrated in Figure 22 was used to collect the wayside acoustic signals. This system included a 16 element linear

microphone array, three pairs of light-gates, a sonic anemometer and recording equipment. The light-gates were used to trigger the recording system and to measure the speed of the train in order to align the audio signals with the position of the bearings. A beamforming algorithm [33,34] was used to remove the Doppler Effect from the signals collected by the wayside acoustic monitoring system. In the experiment, the train took approximately 0.38 seconds to pass through the detection zone. The sampling frequency used was 12500 Hz, and each recoding consisted of 4096 samples. In addition to the recorded faulty signal, a recording of a healthy bearing was also used. The time domain waveforms of both faulty and fault free signals, with the Doppler Effect removed, are shown in Figure 23, and their Hilbert envelope spectra are shown in Figure 24. Figure 24 shows significant levels of background noise, along with two main harmonic components at 30.52 Hz and 61.04 Hz in the Hilbert envelope spectrum for the faulty bearing. These peaks, however, do not correspond to the fault frequencies for this bearing, and as such conventional spectrum analysis is unable to extract the week fault feature from the wayside acoustic signal.

Please insert the Figure 22 into here

Please insert the Figure 23 into here

Please insert the Figure 24 into here

Using the ISVD-RSSD method, the signals recorded during the field experiment and shown in Figure 23 (a) and (b) can be decomposed into high and the low resonance components as shown in Figure 25 and Figure 26 respectively. The parameters used in the ISVD-RSSD method for the field experiment are provided in Table 6. Figure 27 shows the Hilbert envelope spectra of the high resonance components for both the healthy and faulty bearing signals. The figure shows that the two main faulty bearing harmonic components (at 30.52Hz and 61.04Hz) identified using the standard Hilbert envelope analysis are decomposed into the high resonance component. With the harmonic interferences removed, obvious peaks exist at f_{RFF}, $2f_{RFF}$ and $3f_{RFF}$ in the Hilbert envelope spectrum of the low resonance component of

the faulty bearing signal. This is shown in Figure 28 and corresponds to the presence of the roller bearing fault.

Please insert the Table 6 into here

Please insert the Figure 25 into here

Please insert the Figure 26 into here

Please insert the Figure 27 into here

Please insert the Figure 28 into here

As with the laboratory experiment, the significance of the ISVD component of the ISVD-RSSD method can be evaluated. The recorded test signal for the bearing fault, as shown in Figure 25(b), is decomposed using the RSSD method alone and the Hilbert envelope spectrum of the obtained low resonance component is shown in Figure 29. The figure shows many residual noises and harmonic components. Although a peak corresponding to f_{RFF} can be seen, the residual components can still easily result in missed diagnosis. Hence it is considered that the ISVD method is necessary to de-noise the collected signal before using the RSSD method.

Please insert the Figure 29 into here

The test signal, as shown in Figure 23(b), can also be decomposed using ensemble empirical mode decomposition (EEMD). The first intrinsic mode function (IMF) is selected due to it having the maximum kurtosis value and its corresponding time domain waveform is shown in Figure 30(a). The figure shows no obvious peak at f_{RFF} or any of its harmonics. This is likely to result in a missed diagnosis when using the EEMD method.

Please insert the Figure 30 into here

To further verify the effectiveness of the proposed method, an additional field experiment, based on a roller fault, was conducted. The experimental conditions were

the same as in the experiment described above. The time domain waveform and the Hilbert envelope spectrum of the analysis signal are shown in Figure 31 (a) and (b), respectively. The figure shows that there are harmonic components and that there is a high level of noise in the analysis signal.

Please insert the Figure 31 into here

The analysis signal as shown in Figure 31 (a) is subjected to the proposed method and the result is shown in Figure 32. Figure 32 (a) and (b) are the time domain waveform and the Hilbert envelope spectrum of the obtained low resonance component. The figure shows that there are obvious peaks at f_{RFF} and its harmonics, which indicate the existence of a roller fault. Hence, the effectiveness of the proposed method is further demonstrated.

Please insert the Figure 32 into here

Conclusion

In this paper, a novel method based on a combination of the ISVD and RSSD methods is proposed. The ISVD-RSSD method has successfully been used to demonstrate adaptive fault feature extraction of train axle bearing faults from wayside acoustic signals. The RSSD component of the method has been shown to be able to nonlinearly separate the fault signals, which manifest as impacts, from harmonic elements; presenting them in high and low resonance components respectively. This decomposition capability has, however, been shown to be significantly influenced by interference arising from noise within the source signals. Wayside acoustic signals usually include significant levels of noise due to their environment and the surrounding other components of the train. In order to better extract the fault / impact components, ISVD is introduced as a preprocessor to de-noise the wayside acoustic signals.

This paper has also shown that the parameters of the ISVD-RSSD method can be adaptively selected to obtain the best decomposition effect. The method has been

evaluated using both laboratory and field experiments. The following conclusions are obtained through consideration of both tests:

(1) The ISVD method can be used to remove background noise from wayside acoustic signals. Envelope Spectrum Entropy and stepwise optimisation have been introduced as strategies for the adaptive selection of parameters for the S-G filter and have been shown to produce good results. However, the optimisation time for the parameters of the filter are 560 s and 570 s in the laboratory experiment and the field experiment respectively. The efficiency of the optimisation processes in the ISVD method need to be improved as a topic of further research.

(2) The RSSD method has been shown to be appropriate for the exclusion of harmonic components thus allowing the extraction of bearing fault feature signals based on them having different oscillatory behaviour. The adaptive parameter selection method based on GA has been shown to be functional, but also a time-consuming process. Improving the performance of this element will be the focus of further research.

(3) The ISVD-RSSD method has been compared to the conventional spectrum analysis and EEMD approaches. When used for the detection of faults in train axle bearings from wayside acoustic signals, the results indicate significant performance improvements when using the ISVD-RSSD method.

Acknowledgements

This study was supported by the China Scholarship Council and the Guangzhou Science and Technology Plan (Ref. 201508030038), and makes use of data recorded during previous studies sponsored by Hitachi Rail Europe. The authors would like to express their gratitude to Rail Alliance and Motorail Logistics for providing access to their test facilities. The authors would also like to acknowledge guidance provided by Ivan Selesnick on the TQWT toolkit.

References

[1] X. Yan , C. Zhao, Z. Lu, X. Zhou, H. Xiao , A study of information technology used in oil monitoring, Tribol Int, 38 (2005) 879-886.

[2] H. Cao , F. Fan, K. Zhou, Z. He, Wheel-bearing fault diagnosis of trains using empirical wavelet transform, Measurement, 82 (2016) 439-449.

[3] Z. Zhang, M. Entezami, E. Stewart, C. Roberts, Enhanced fault diagnosis of roller bearing elements using a combination of empirical mode decomposition and minimum entropy deconvolution, Proc. Inst. Mech. Eng. Part C-J. Eng. Mech. Eng. Sci. 231 (2017) 655-671.

[4] A. Amini, M. Entezami, Z. Huang, H. Rowshandel, M. Papaelias, Wayside detection of faults in railway axle bearings using time spectral kurtosis analysis on high-frequency acoustic emission signals, Adv. Mech. Eng. 8 (2016) 1-9.

[5] H. Deilamsalehy, T. C. Havens, P. Lautala, E. Medici, J. Davis, An automatic method for detecting sliding railway wheels and hot bearings using thermal imagery, Proc. Inst. Mech. Eng. Part F-J. Rail Rapid Transit. 231 (2017) 690-700.

[6] J. Robert, Railway bearings: an investigation of causes of hot boxes in railway service, and methods for their prevention, J. Franklin Inst. 149 (1900) 439-450.

[7] T. David, Railway noise and vibration: mechanisms, modelling and means of control, Elsevier, 2008.

[8] C. Wang , F. Hu , Q. He, A. Zhang , F. Liu, F. Kong , De-noising of wayside acoustic signal from train bearings based on variable digital filtering, Appl. Acoust. 83 (2014) 127-140.

[9] Q. He , J. Wang, F. Hu, F. Kong , Wayside acoustic diagnosis of defective train bearings based on signal resampling and information enhancement, J. Sound Vibr. 332 (2013) 5635–5649.

[10] H. Zhang , S. Zhang , Q. He, F. Kong , The Doppler Effect based acoustic source separation for a wayside train bearing monitoring system, J. Sound Vibr. 361 (2016) 307–329.

[11] I. W. Selesnick , Resonance-based signal decomposition: A new sparsity-enabled signal analysis method, Signal Process. 91 (2011) 2793–2809.

[12] D. Zhang, D. Yu, X. Li, Optimal resonance-based signal sparse decomposition and its application to fault diagnosis of rotating machinery, Proc. Inst. Mech. Eng. Part C-J. Eng. Mech. Eng. Sci. 24 (2017) 4670-4683.

[13] D. Zhang, D. Yu, W. Zhang , Energy operator demodulating of optimal resonance components for the compound faults diagnosis of gearboxes, Meas. Sci. Technol. 26 (2015) 115003

[14] J. Luo , D. Yu, M. Liang, Enhancement of oil particle sensor capability via resonance-based signal decomposition and fractional calculus, Measurement. 76 (2015) 240-254.

[15] H. Wang, J. Chen, G. Dong, Feature extraction of rolling bearing's early weak fault based on EEMD and tunable Q-factor wavelet transform, Mech. Syst. Signal Proc. 48 (2014) 103-119.

[16] H. Hassanpour , Improved SVD-based technique for enhancing the time-frequency representation of signals, in 2007 IEEE International Symposium on Circuits and Systems, New Orleans, 2007.

[17] H. Hassanpour, A. Zehtabian, S. Sadati, Time domain signal enhancement based on an optimized singular vector denoising algorithm, Digit. Signal Prog. 22 (2012) 786-794.

[18] J. Chen , Y. Zi , Z. He, J. Yuan , Compound faults detection of rotating machinery using improved adaptive redundant lifting multiwavelet, Mech. Syst. Signal Proc. 38 (2013) 36–54.

[19] J. Sun , Q. Xiao , J. Wen, F. Wang, Natural gas pipeline small leakage feature extraction and recognition based on LMD envelope spectrum entropy and SVM, Measurement. 55 (2014) 434–443.

[20] Z. A. Putra, K. A. Amminudin, Two-Step Optimization Approach for Design of A Total Water System, Ind. Eng. Chem. Res. 47 (2008) 6045-6057.

[21] F. Santini , L. Alberotanza , R. M. Cavalli , S. Pignatti, A two-step optimization procedure for assessing water constituent concentrations by hyperspectral remote sensing techniques: An application to the highly turbid Venice lagoon waters, Remote Sens. Environ. 114 (2010) 887–898.

[22] K. L. Jusko, W. P. Shively, Applying a Two-Step Strategy to the Analysis of Cross-National Public Opinion Data, Polit. Anal. 13 (2005) 327-344.

[23] H. Jiang , J. Chen , G. Dong , T. Liu, G. Chen , Study on Hankel matrix-based SVD and its application in rolling element bearing fault diagnosis, Mech. Syst. Signal Proc. 52 (2015) 338–359.

[24] D. M. Bart, The singular value decomposition and long and short spaces of noisy matrices, IEEE Trans. Signal Process. 41 (1993) 2826-2838.

[25] M. Liang, I. S. Bozchalooi, An energy operator approach to joint application of amplitude and frequency-demodulations for bearing fault detection, Mech. Syst. Signal Proc. 24 (2010) 1473-1494.

[26] L. Cao, Practical method for determining the minimum embedding dimension of a scalar time series, Physica D. 110 (1997) 43-50.

[27] Y. Liu , Q. Qian , Y. Fu , F. Liu, S. Lu , Wayside acoustic fault diagnosis of railway wheel-bearing paved with Doppler Effect reduction and EEMD-based diagnosis information enhancement, in 10th International Conference on Sensing Technology (ICST), Nanjing, 2016.

[28] N. Hu, C. Min, W. Wen, The application of stochastic resonance theory for early detecting rub-impact fault of rotor system, Mech. Syst. Signal Proc. 17 (2003) 883-895.

[29] X. Zhao, B. Ye, Selection of effective singular values using difference spectrum and its application to fault diagnosis of headstock, Mech. Syst. Signal Proc. 25 (2011) 1617–1631.

[30] J. Bobin , J.L. Starck, J. M. Fadili , Y. Moudden, D. L. Donoho, Morphological component analysis: an adaptive thresholding strategy, IEEE Trans. Image Process. 16 (2007) 2675-2681.

[31] M. V. Afonso , J. M. Bioucas-Dias, M. A. T. Figueiredo , An augmented Lagrangian approach to the constrained optimization formulation of imaging inverse problems, IEEE Trans. Image Process. 20 (2011) 681-695.

[32] S. I. W. , "TQWT toolbox guide," Electrical and Computer Engineering, Polytechnic Institute of New York University, 2011. http://eeweb. poly. edu/iselesni/TQWT/index. html.

[33] M. Entezami , E. Stewart , J. Tutcher , W. Driscoll , R. Ellis , G. Yeo , Z. Zhang , C. Roberts , T. Kono, S. Bayram , Acoustic analysis techniques for condition monitoring of roller bearings. in Railway Condition Monitoring, in 6th IET Conference on Railway Condition Monitoring (RCM 2014) , Birmingham, 2014.

[34] G. Zechel, A. Zeibig, M. Beitelschmidt, Time-domain beamforming on moving objects with known trajectories, in Berlin Beamforming Conference (BeBeC), Berlin , 2010.

[35] I. W. Selesnick , Resonance-based signal decomposition: A new sparsity-enabled signal analysis method, Signal Process, 91 (2011) 2793–2809.

[36] X. P. Yan, C. H. Zhao, Z. Y. Lu, X. C. Zhou, H. L. Xiao. A study of information technology used in oil monitoring. Tribol. Int. 38 (2005) 879-886.

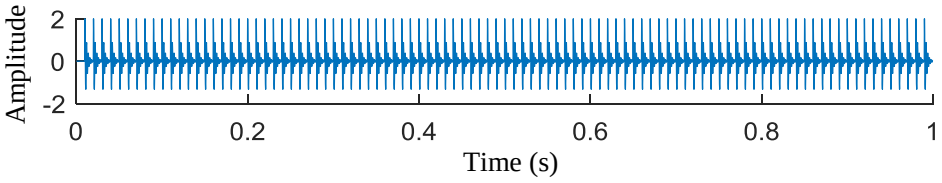

Figure 1: Simulated fault feature signal

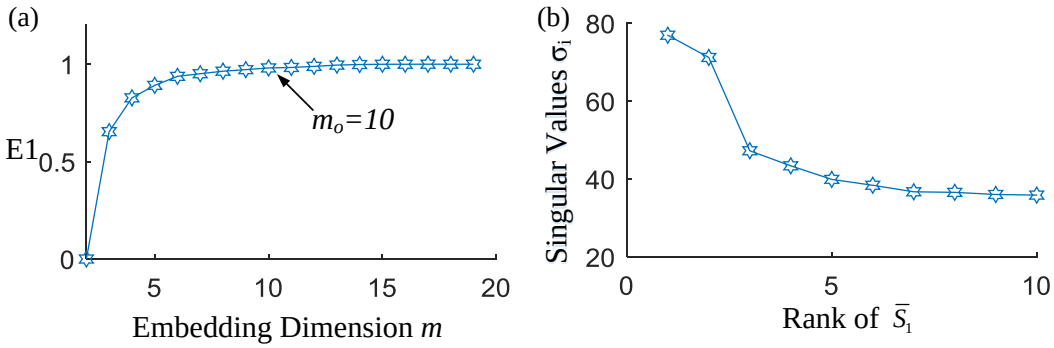

Figure 2: (a) Optimal embedding dimension (b) singular values

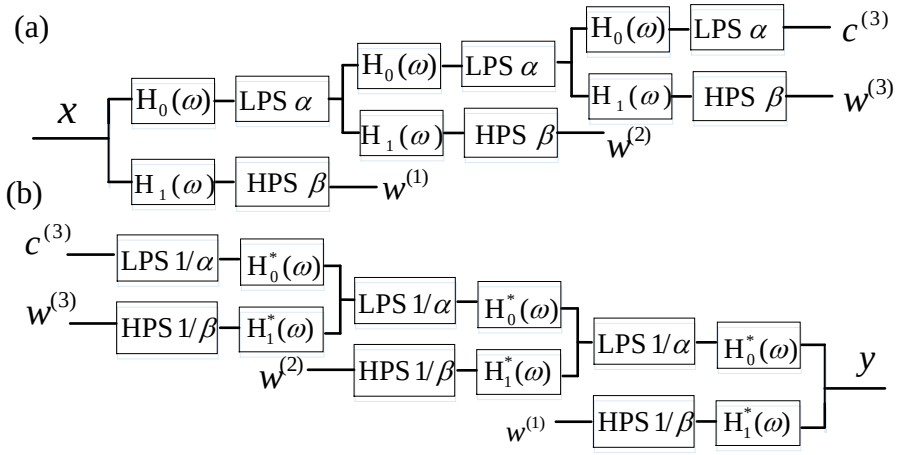

Figure 3: Tunable-Q wavelet transforms: (a) the analysis filter banks (b) the synthesis filter banks

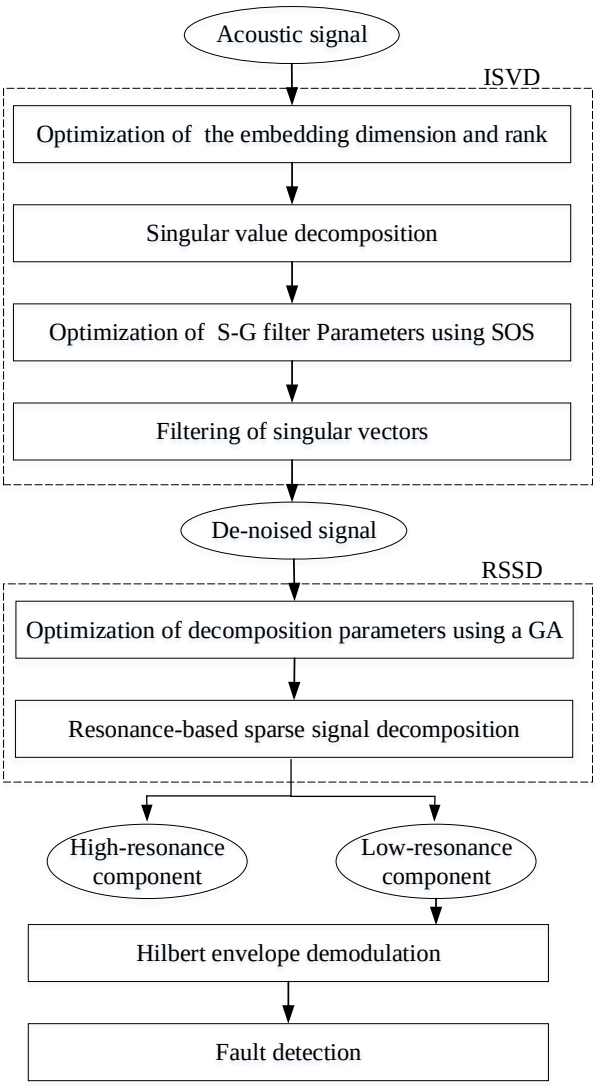

Figure 4: Flow chart describing the proposed method

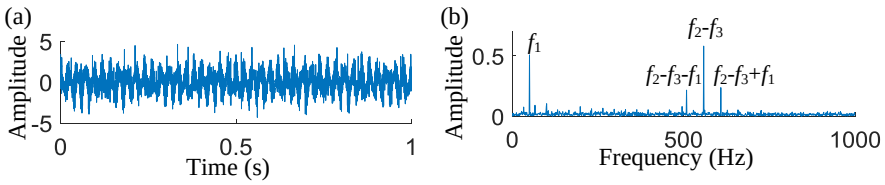

Figure 5: The time domain waveform and the Hilbert envelope spectrum of the synthesized signal. (a) time domain waveform; (b) Hilbert envelope spectrum.

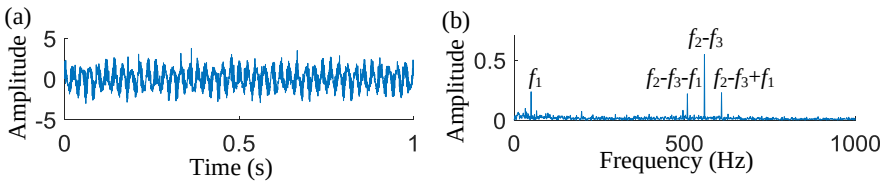

Figure 6: The time domain waveform and the Hilbert envelope spectrum of the denoised signal in simulation experiment. (a) time domain waveform; (b) Hilbert envelope spectrum.

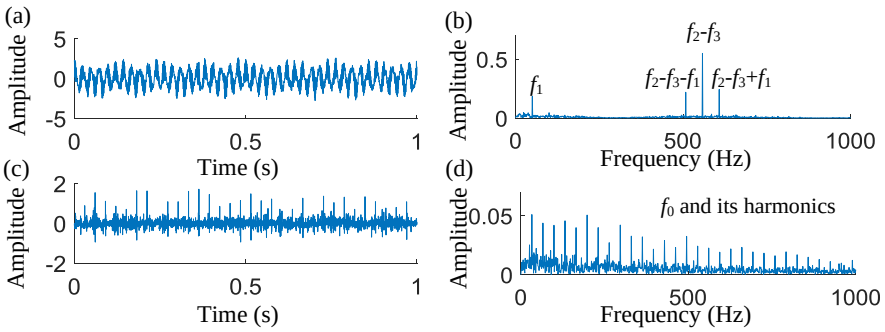

Figure 7: The result of the RSSD method for the denoised signal. (a) time domain waveform of high resonance component and (b) its Hilbert envelope spectrum; (c) time domain waveform of low resonance component and (d) its Hilbert envelope spectrum.

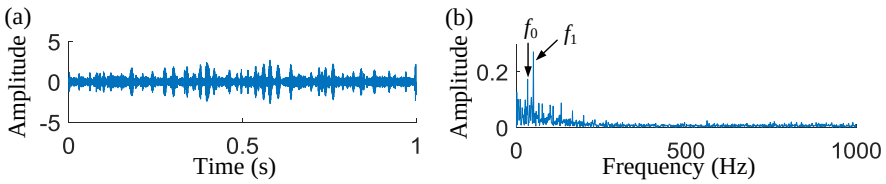

Figure 8: EEMD analysis of synthesized signal (a) Time domain waveform of second IMF (b) Corresponding Hilbert envelope spectrum

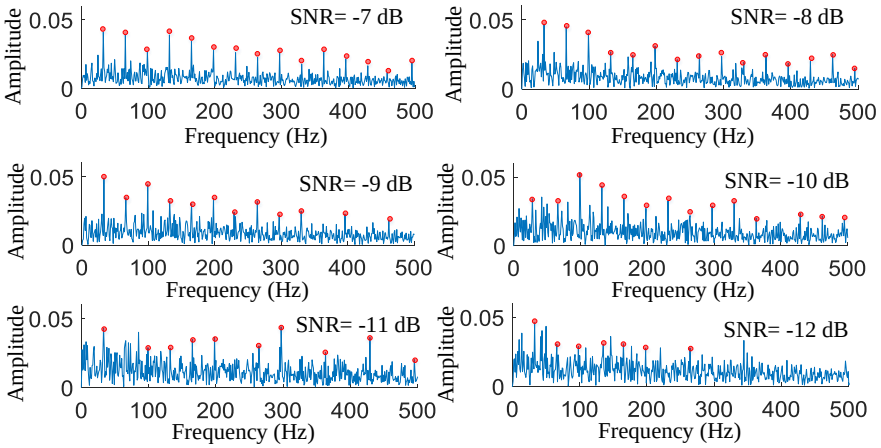

Figure 9: Influence of noise on the proposed method

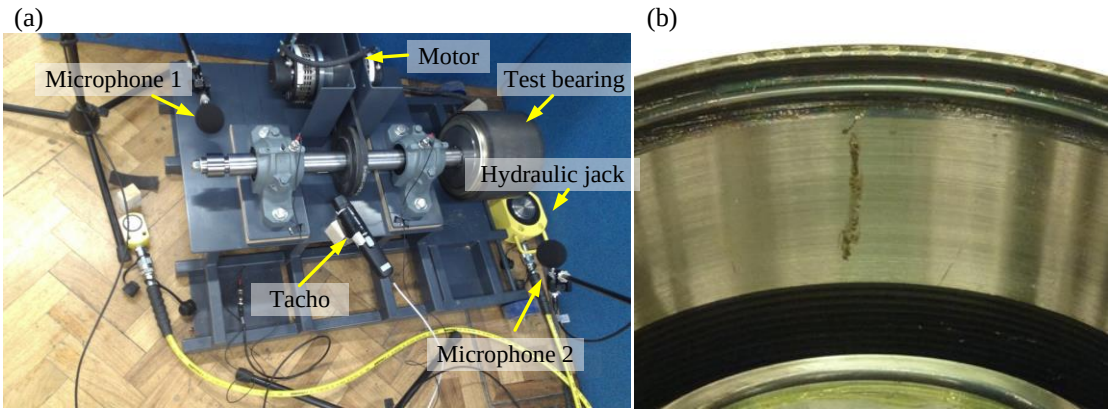

Figure 10: Test rig and test bearing with outer race fault

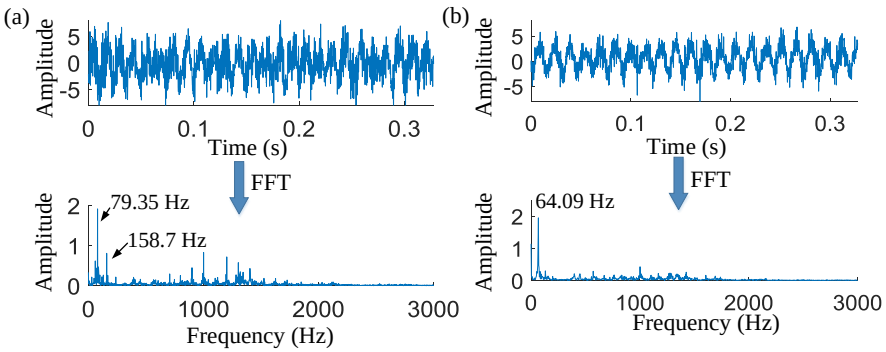

Figure 11: Time domain waveform of signals recorded in the laboratory experiment and corresponding FFT spectra (a) healthy bearing (b) faulty bearing

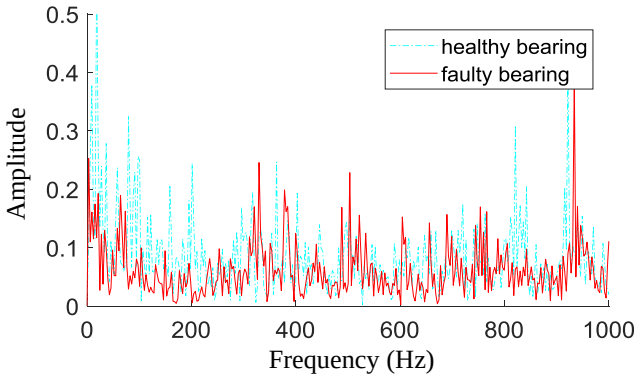

Figure 12: Hilbert envelope spectra of signals recorded in the laboratory experiment

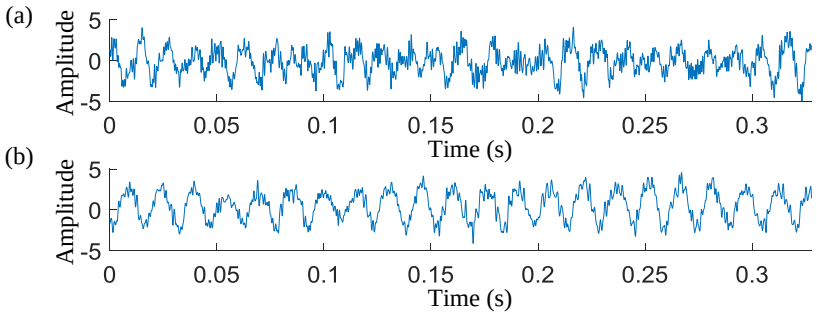

Figure 13: Time domain waveform of the de-noised signals (a) healthy bearing (b) faulty bearing

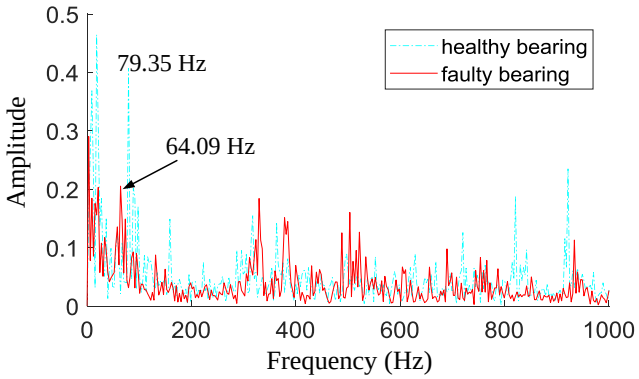

Figure 14: Hilbert envelope spectra of the de-noised signals

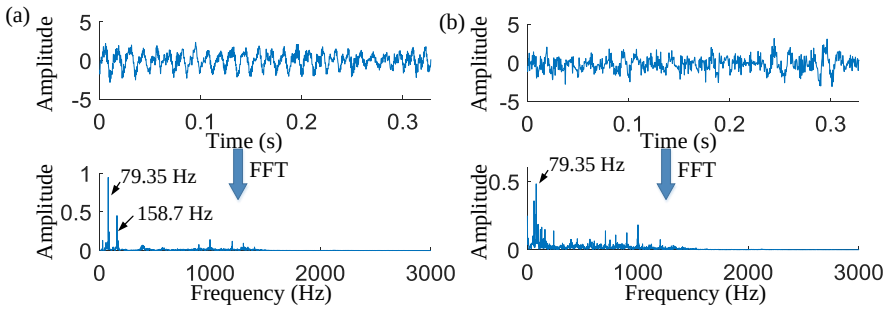

Figure 15: Time domain waveforms and FFT spectra of resonance components for healthy bearing (a) high resonance component (b) low resonance component

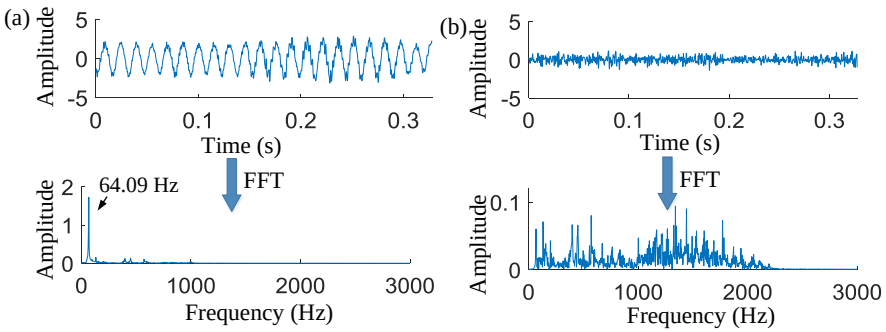

Figure 16: Time domain waveform and FFT spectra of resonance components for faulty bearing (a) high resonance component (b) low resonance component

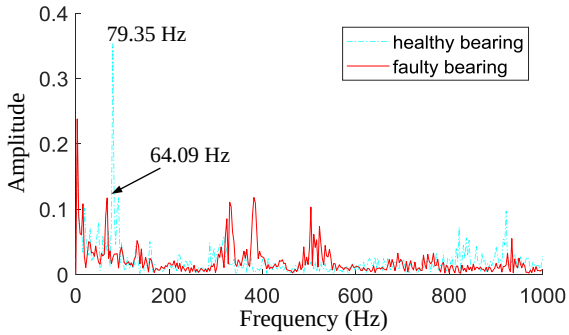

Figure 17: Hilbert envelope spectra of the high resonance component

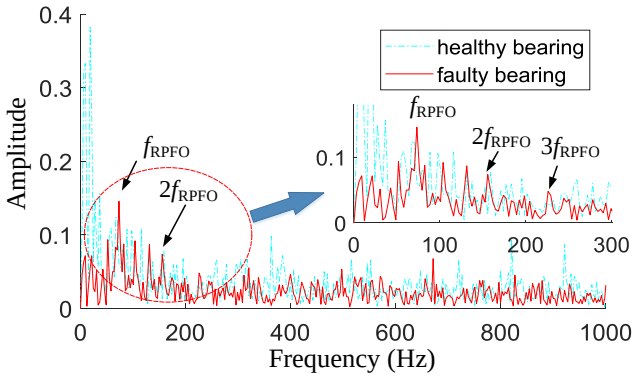

Figure 18: Hilbert envelope spectra of the low resonance component

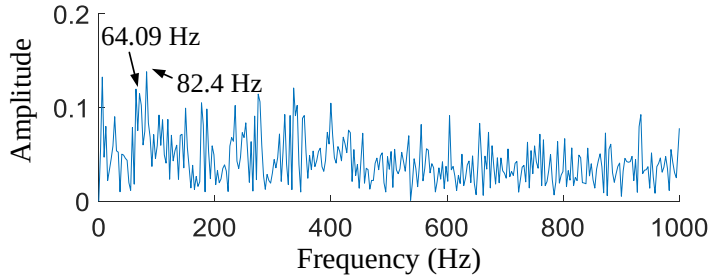

Figure 19: Hilbert envelope spectrum of the low resonance component of the raw signal

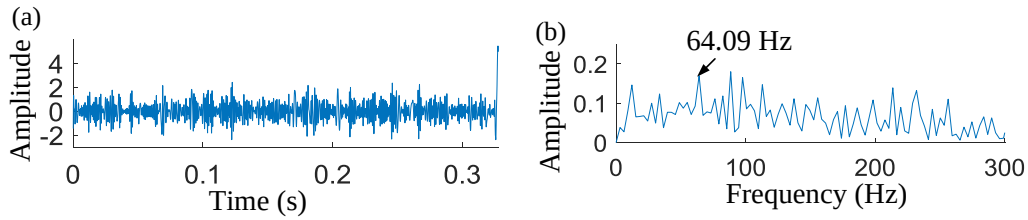

Figure 20: EEMD analysis of the test signal recorded from the faulty bearing (a) Time domain waveform of second IMF (b) Corresponding Hilbert envelope spectrum

(a)

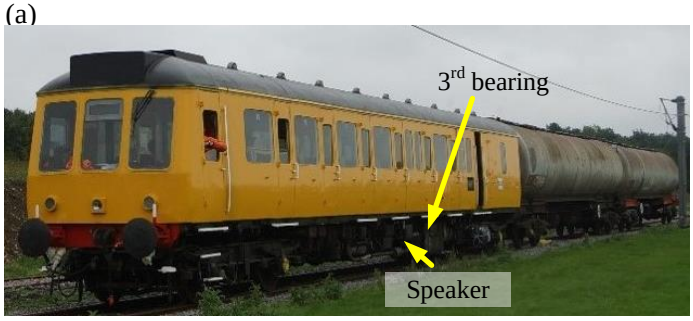

(b)

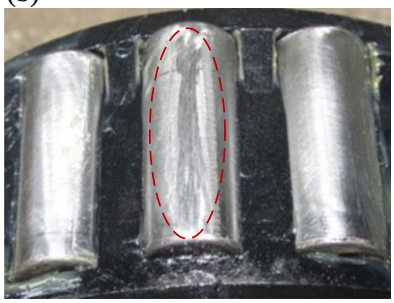

Figure 21: (a) Test train. (b) Test bearing with roller fault

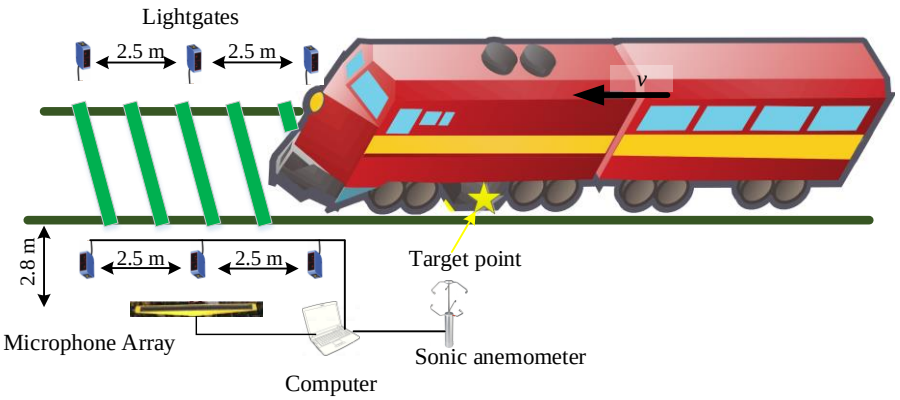

Figure 22: Overview of the wayside acoustic monitoring system

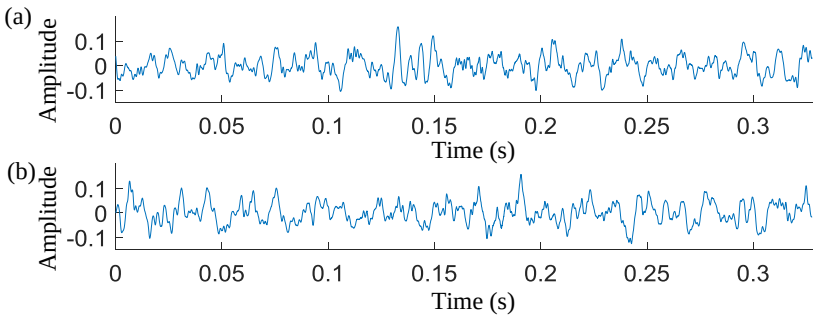

Figure 23: Time domain waveforms of test signals (a) healthy bearing (b) faulty bearing

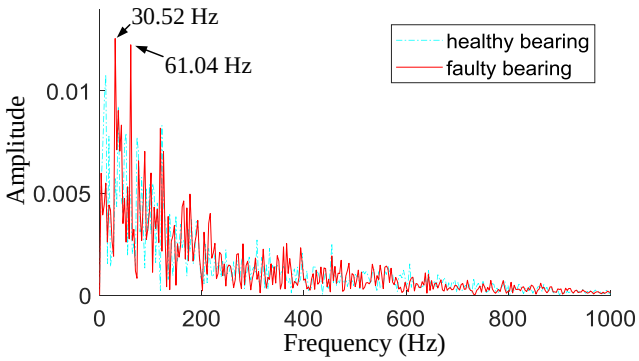

Figure 24: Hilbert envelope spectra of the test signals recorded during the field experiment

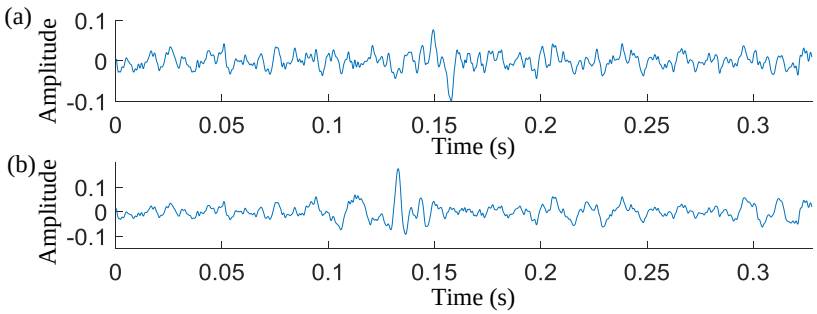

Figure 25: Time domain waveforms of resonance components for the healthy bearing (a) high resonance component (b) low resonance component

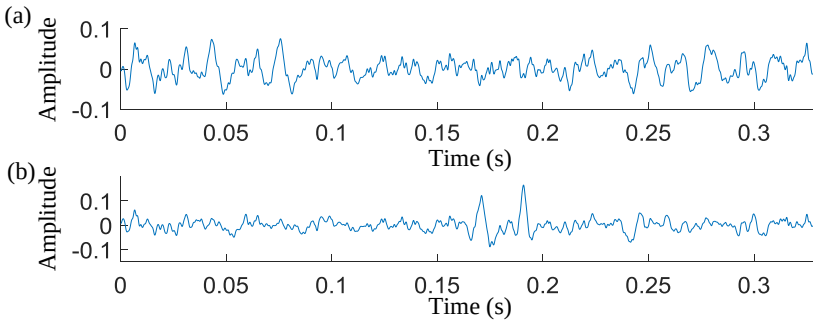

Figure 26: Time domain waveforms of resonance components for the faulty bearing (a) high resonance component (b) low resonance component

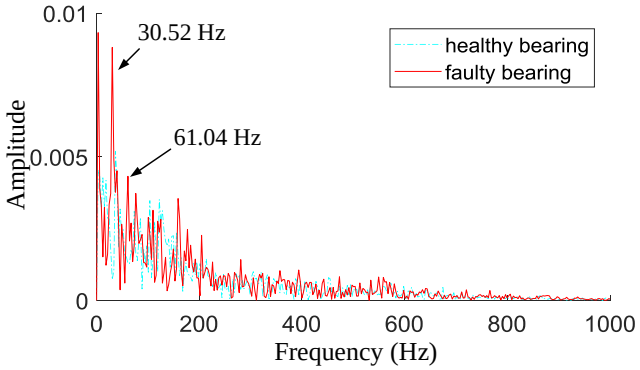

Figure 27: Hilbert envelope spectra of the high resonance components

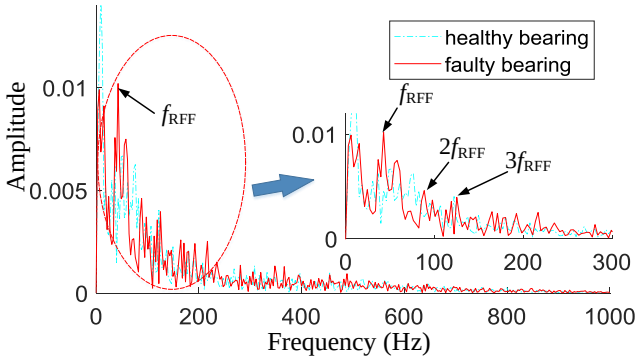

Figure 28: Hilbert envelope spectra of the low resonance components

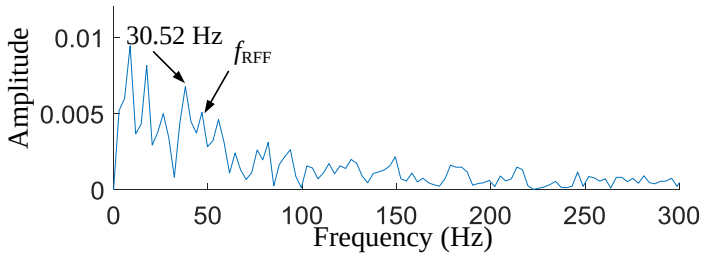

Figure 29: Hilbert envelope spectrum of the low resonance component

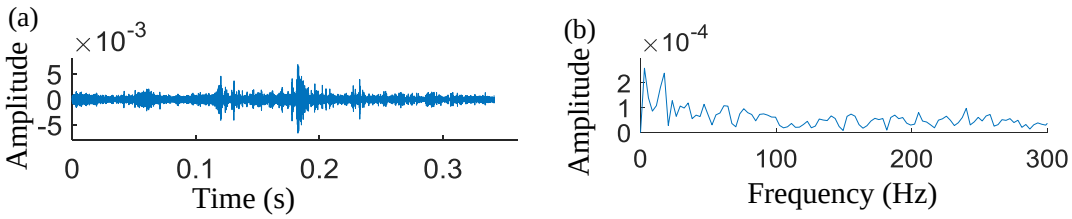

Figure 30: EEMD analysis of the test signal from the faulty bearing (a) Time domain waveform of first IMF (b) Corresponding Hilbert envelope spectrum

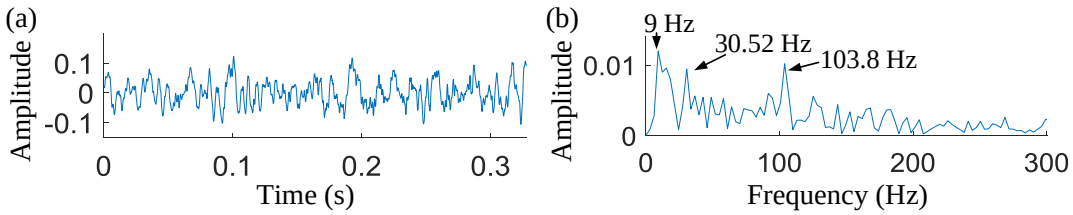

Figure 31 The analysis signal including roller fault information (a) Time domain waveform (b) Hilbert envelope spectrum

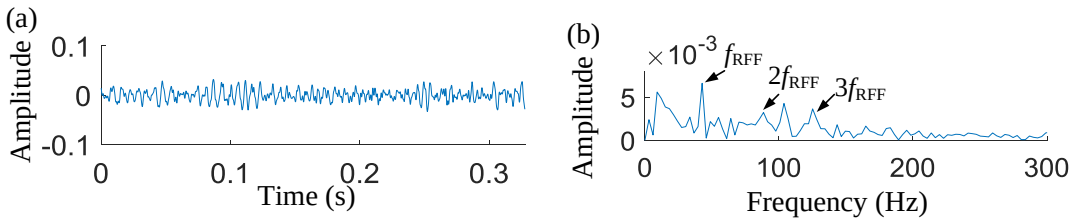

Figure 32 The obtained low resonance component for the analysis signal (a) Time domain waveform (b) Hilbert envelope spectrum

Table 1 Parameters of the simulation signal

M	A_m	β	f_{re}	T
50	1	-420	520 Hz	1/100 s

Table 2 De-noising results for the conventional methods and the ISVD method

	Signal1	Signal2	Signal3	Signal4
$SNR_{Original}$	-15 dB	-10 dB	-5 dB	0 dB
SNR_{SVD}	-7.3 dB	-5.18 dB	-0.98 dB	2.58 dB
SNR_{LPSR}	-6.73 dB	-5.09 dB	-3.42 dB	0.76 dB
SNR_{EEMD}	-4.82 dB	-2.76 dB	- 0.62 dB	1.06 dB
SNR_{ISVD}	-3.53 dB	1.05 dB	3.38 dB	4.35 dB

Table 3 Test bearing parameters

Type	Number of rollers n	Roller diameter RD	Pitch diameter PD	Contact angle B
801023AB	21	5.3 mm	42.5 mm	13.8^{o}

Table 4 ISVD-RSSD parameters used in the laboratory experiment

	m	d	n_W	Q_1	r_1	Q_2	r_2
Healthy	8	3	5	6.25	9.12	1.07	3.07
Faulty	8	3	15	13.99	4.04	2.8	3.27

Table 5 Test bearing parameters in field experiment

Type	Number of rollers n	Roller diameter RD	Pitch diameter PD	Contact angle B
TAROL 130/230-U-TVP	22	24 mm	187 mm	6.9^{o}

Table 6 parameters for the ISVD-RSSD method used in the field experiment

	m	d	n_W	Q_1	r_1	Q_2	r_2
Healthy	6	4	23	32.46	27.66	1.81	3.19
Faulty	4	4	23	5.76	4.69	1	4.43